# UC Irvine
## UC Irvine Previously Published Works


### Title
Atomic Force Microscopy Investigation of Viruses


### Permalink
https://escholarship.org/uc/item/7ps6t0r8



### Authors
McPherson, Alexander
Kuznetsov, Yurii G



### Publication Date
2011

### DOI
10.1007/978-1-61779-105-5_12



### Copyright Information
This work is made available under the terms of a Creative Commons Attribution License, availalbe at https://creativecommons.org/licenses/by/4.0/

Peer reviewed

eScholarship.org Powered by the California Digital Library
University of California

# Chapter 12

# Atomic Force Microscopy Investigation of Viruses

**Alexander McPherson and Yurii G. Kuznetsov**

## Abstract

Atomic force microscopy (AFM) has proven to be a valuable approach to delineate the architectures and detailed structural features of a wide variety of viruses. These have ranged from small plant satellite viruses of only 17 nm to the giant *mimivirus* of 750 nm diameter, and they have included diverse morphologies such as those represented by HIV, icosahedral particles, *vaccinia*, and bacteriophages. Because it is a surface technique, it provides images and information that are distinct from those obtained by electron microscopy, and in some cases, at even higher resolution. By enzymatic and chemical dissection of virions, internal structures can be revealed, as well as DNA and RNA. The method is relatively rapid and can be carried out on both fixed and unfixed samples in either air or fluids, including culture media. It is nondestructive and even non-perturbing. It can be applied to individual isolated virus, as well as to infected cells. AFM is still in its early development and holds great promise for further investigation of biological systems at the nanometer scale.

**Key words:** Imaging, Nanoscale, Structure, Infection, Nucleic acids, Icosahedra

## 1. Introduction

A direct imaging technology that promises to have a significant impact on structural biology, and which is, in most ways, complementary to X-ray diffraction and electron microscopy, the classical approaches, is atomic force microscopy (AFM) (1–3). An immediate advantage of AFM is that it is based on relatively simple physical principles, unlike X-ray crystallography, and the instruments are mechanically and electronically rather straightforward, unlike electron microscopy. Unlike both of the other technologies, AFM is fairly inexpensive to institute and apply, even to biological specimens. The acuity and investigative size range of the AFM have proven to be quite remarkable and it is now permitting researchers new access to virus structure and the effects of viruses on organisms. Indeed, it has allowed us to

Pier Carlo Braga and Davide Ricci (eds.), *Atomic Force Microscopy in Biomedical Research: Methods and Protocols*, Methods in Molecular Biology, vol. 736, DOI 10.1007/978-1-61779-105-5_12, © Springer Science+Business Media, LLC 2011

visualize the surface features, internal structures, and the nucleic acid cores of many viruses. At the same time, it has proven to be an effective instrument for observing viruses emerging from animal cells, and the perturbations they produce to the cells.

## 2. Materials

1. Glutaraldehyde for sample fixation was made by diluting a commercial solution to a concentration of 5% w/v with distilled water, and kept in a light-free container. Glutaraldehyde should be freshly prepared at least every 2 weeks and maintained at 4°C.
2. Poly-L-lysine for coating cover slips was prepared by dissolving lyophilized polymer in distilled water to a final concentration of 1 mg/ml. This stock solution, maintained at 4°C, was further diluted to 0.1 mg/ml before application to substrates.
3. Magnesium and nickel chloride for treating substrates were made by dissolving reagent-grade salts in distilled water to concentrations of 50 mM.
4. Substrates for AFM were acid-washed glass or plastic, 1-cm diameter cover slips, which were extensively rinsed with distilled water. Alternately, the substrates were freshly cleaved mica.
5. Virus samples were diluted from their stocks into distilled water when possible, and into phosphate-buffered saline otherwise. Substrates with samples, unless air-dried directly, were rinsed with distilled water before air drying.
6. For scanning in fluids, the fluid cell was filled with either distilled water or phosphate-buffered saline.
7. Any other reagents, such as enzymes, detergents, or reducing agents, were prepared from the highest grade materials available and dissolved in distilled water or phosphate-buffered saline. These were maintained at –20°C in small aliquots and thawed for use as needed.

## 3. Methods

### *3.1. AFM Instrument Setup*

AFM instruments can be operated in either contact mode, or what is referred to as tapping mode. In contact mode, a probe made of silicon or silicon nitride is placed in near contact with the surface of interest, say the capsid of a virus, and then translated in a systematic raster mode over the surface. The AFM probe is a

sharp stylus similar in function to a minute phonograph needle. The tip ideally has a single point, with a very small radius of curvature. The probe is mounted at the end of a short cantilever, typically 100–250 μm in length, which has a low spring constant to minimize the force between the tip and the sample.

Scanning is achieved by translating the sample beneath the probe, using a piezoelectric positioned x–y stage, along a continuous sequence of raster lines. As the probe tip passes over the surface, it interacts through "aggregate atomic forces," which remain somewhat mysterious, with structural features on the surface. Encounters with these substructures cause the probe to be displaced vertically as the tip rides across. Exceedingly small displacements of the tip are amplified by deflection of a laser beam that is reflected from the upper surface of the cantilever, and these deflections are detected and tracked by a split photodiode. Photoelectric circuitry converts the deflections into height information. The resulting scan data, recorded as a digital topographical image, can then be presented in a number of visual formats.

Sample perturbation and other problems arising from unfavorable probe–surface interactions have been obviated to a great extent by the development of "tapping" mode instruments (4). With tapping mode, the probe tip is not in continuous contact with the sample surface, but rapidly oscillates up and down as it is scanned over the surface, essentially "tapping" its way and gently sensing the heights of obstacles it encounters. In tapping mode, the vertical position of the sample is continually adjusted by a feedback mechanism to maintain the amplitude of the freely oscillating probe constant (see Note 1).

The "tapping mode" approach has proven to be a significant boon in biological investigations as it has allowed the characterization of samples that would otherwise be too soft or too fragile to withstand contact mode examination. Operating with tapping mode in a liquid environment presents some complications due to fluid dynamics, but these are not severe. A constraint that sometimes presents obstacles during analysis in a liquid medium is that the specimen under study must be fixed to, or made to adhere firmly to the substrate surface of the fluid cell, which may be glass, cleaved mica, plastic, or any other hard material (see Note 2).

One particular feature of AFM must be borne in mind whenever one is interpreting images. The one- or two-dimensional profile obtained of any object, or surface substructure, is the convolution of the tip shape with that of the feature being scanned. This is illustrated in Fig. 1. An image of an object scanned with a broad, dull tip is not the same as that acquired with a sharper tip. In particular, while the height of the object will be the same regardless of the tip shape (because the maximum vertical deflection of the cantilever tip would be the same), the lateral dimensions will not. A broader tip yields a broader object, and a sharper tip produces the more accurate size (see Note 3). Whereas height information is almost

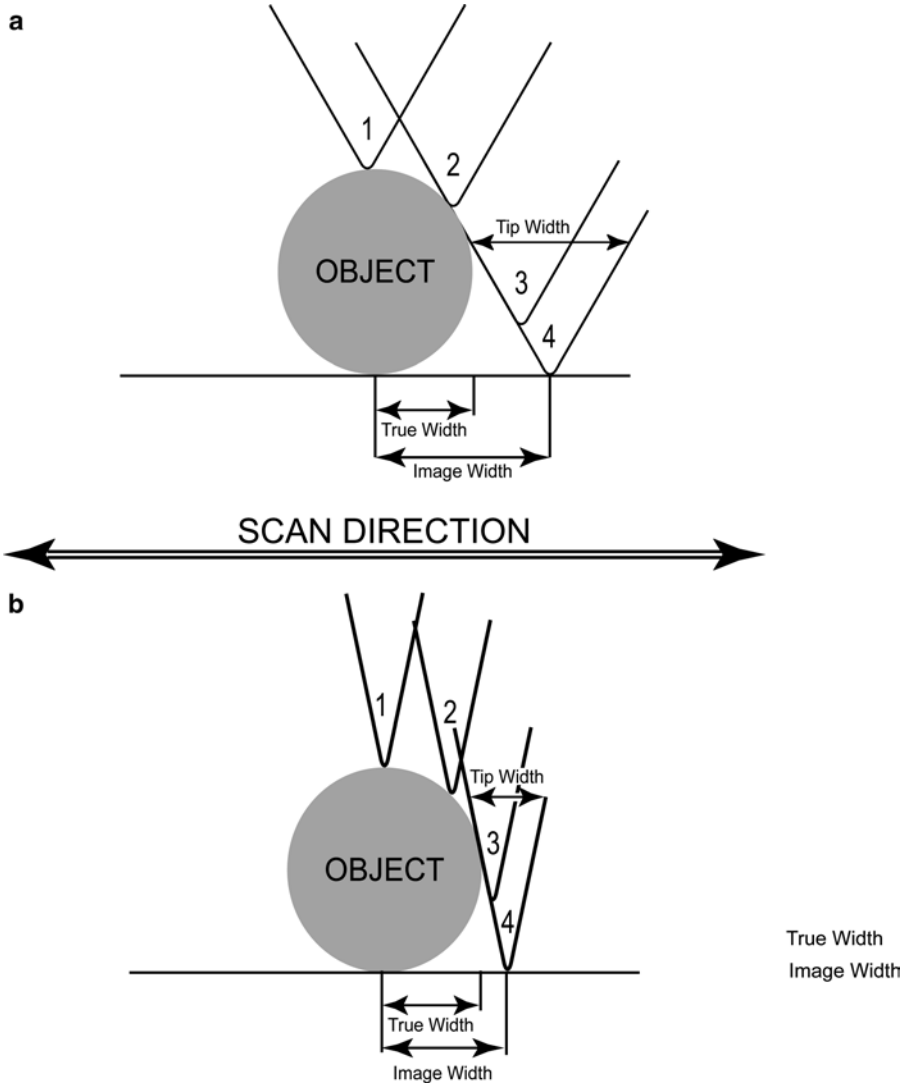


Fig. 1. Schematic illustration of the convolution of the shape of the AFM tip with the shape of the feature, or particle being scanned. The side of the cantilever tip contacts the object and begins to produce a deflection of the cantilever before the tip apex actually reaches the object. Similarly, the opposite side of the tip is still in contact with the object even after the apex itself has passed. Thus the total deflection implies a virtual lateral dimension for the object greater than its actual dimension. The difference between the virtual and actual dimensions is a function of the width of the cantilever tip. The sharper the tip, the more accurate the observed dimensions, and the greater the resolution attainable.

always trustworthy, lateral measurements are frequently suspect. The reliability of lateral measurements can, however, be increased if some standard having defined spatial features is first scanned and its known spacings or cell dimensions compared with those in the image. Such standards may be etched grids on silicon, or the surfaces of protein crystals (5). Height resolution for all samples is typically better than 1 nm (see Notes 4–6).

Specimens, however, are not always best visualized under physiological conditions, particularly when high resolution is desired.

Because cantilever tip pressure, even in "tapping mode," may produce deformation, for example, of a cell membrane, in some cases fixation is the better option. This, as with light microscopy histological procedures, usually relies on glutaraldehyde, paraformaldehyde, or osmium tetroxide fixation, followed by dehydration and imaging in water–alcohol mixtures, or in air. These methods have been developed by microscopists for more than a century to preserve the natural morphology of a sample but still allow high-resolution imaging. While not as ideal as *in situ* observation, the cells are no longer alive or viruses infective, fine details of their structures can be visualized that would otherwise be obscured by membrane flexion.

### 3.2. Virus Imaging

The resolution of AFM, in the best of cases, is roughly that of current cryo-EM models (6). It is applied to individual particles and does not yield an average structure over an entire population as do many EM reconstructions. It does not require that a virus have symmetrical or uniform architecture, or even that all particles be the same in structure. Thus, it is equally applicable to small icosahedral viruses such as *tomato bushy stunt virus*, helical viruses such as *tobacco mosaic virus*, and completely irregular, complex viruses such as *vaccinia* or the retroviruses. There is no size restriction. It has been used to analyze small plant viruses such as *turnip yellow mosaic virus* (TYMV) (7) to massive icosahedral viruses such as *PBCV-1*, an algal virus (8), to *mimivirus* (9), the largest virus known.

Viruses were first visualized by AFM in their crystalline form (7, 10, 11), as illustrated by Fig. 2, rather than as single isolated particles, in investigations of the growth of crystals of *satellite tobacco mosaic virus* (STMV) and TYMV (12–14). Because they were immobilized on the surfaces of crystals, conditions were suitable for direct imaging of even the small 17–30-nm diameter

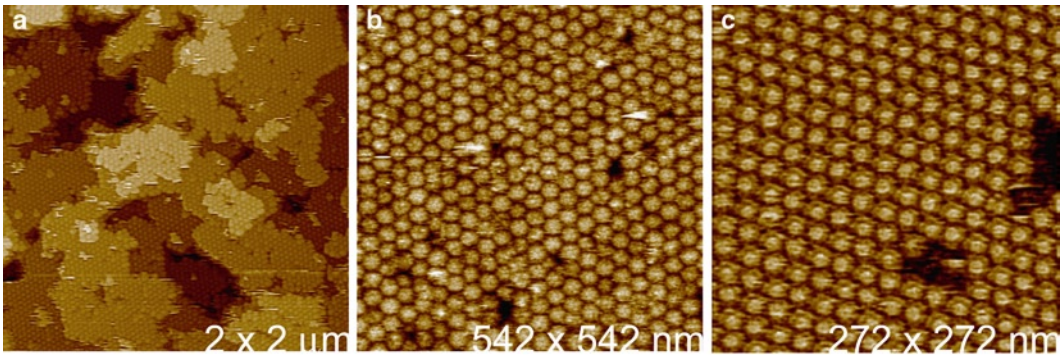


Fig. 2. In (**a**), a low magnification AFM image shows the two-dimensional growth islands that characterize the surfaces of orthorhombic $T=3$ Brome Mosaic Virus (BMV) crystals. In (**b**) is a high magnification AFM image of the surface of the same crystal. As with most virus crystals, vacancies frequently occur in clusters to produce large defects. In (**c**) is a low magnification AFM image of the reassembled $T=1$ particles of BMV in a *tetragonal lattice*. The scan areas are (**a**) 2 µm × 2 µm, (**b**) 542 nm × 542 nm, (**c**) 272 nm × 272 nm.

virions. Larger icosahedral plant viruses in crystalline form were studied subsequently (15–19). The first AFM studies of noncrystalline viruses were retroviruses on cell surfaces (20–22), again, principally because they were immobilized by their association with cell surfaces. Single particles of larger viruses, and helical viruses, were eventually visualized by AFM, and these included tobacco mosaic virus, *cauliflower mosaic virus*, *Tipula iridescent virus* (15, 23), *herpes simplex virus* (24), vaccinia virus (25, 26), and mimivirus (9). Although virus crystals were investigated using both contact and tapping mode, noncrystalline specimens were imaged exclusively with tapping mode, in both air and buffer.

### 3.3. Internal Structure Imaging

Because AFM images the surfaces of specimens, it might be thought that AFM would be of little use in visualizing the interior features of viruses or cells. This, however, is not the case. As has been shown in AFM investigations of a number of viruses, it is, in fact, an invaluable tool for deducing the interior architecture of virions, regardless of their external form or size. This is because it is possible to strip away layers of structure systematically by chemical, physical, and enzymatic means (23, 26, 27) and to accompany this process of dissection by AFM visualization. Using the same strategy as that used by conventional anatomists, it has been proven possible to disassemble viral specimens, see what is inside, and ascertain how the components are linked.

### 3.4. Rapid Shape Classification

A valuable qualitative result that emerges almost immediately from AFM images is what the virus looks like, what is its overall architecture, and how similar are particles to one another. Are they uniformly the same in appearance, or are there a variety of forms? Thus even a cursory investigation may quickly reveal certain general features that allow rapid classification. This is illustrated by the various structural classes of viruses shown in Fig. 3. The virions may be spherical, cylindrical, or filamentous. They may have symmetrically arranged capsomeres or other surface units, fibers, protruding vertices, prolate or icosahedral shapes, unusual morphologies, pleiomorphic character, etc. Tail assemblies may be observed directly, as on phages for example. AFM is, therefore, a useful tool for simply deducing the kind of virus one is dealing with, whether more than one kind of virus is present in a population, and the general level of contamination that may accompany the virus as a consequence – cellular material, degraded virions, and macromolecular impurities of all sorts.

### 3.5. Quantitative Dimensional Measurements

A fundamental parameter for virus particles is their diameter if they are spherical viruses, or their diameter and length if they are helical. AFM can provide measures of these in both the hydrated and dried states, which also gives an estimate of the degree of shrinkage they undergo as a result of dehydration. Because of the finite tip size, and tip-to-tip variation in radius of curvature, it is

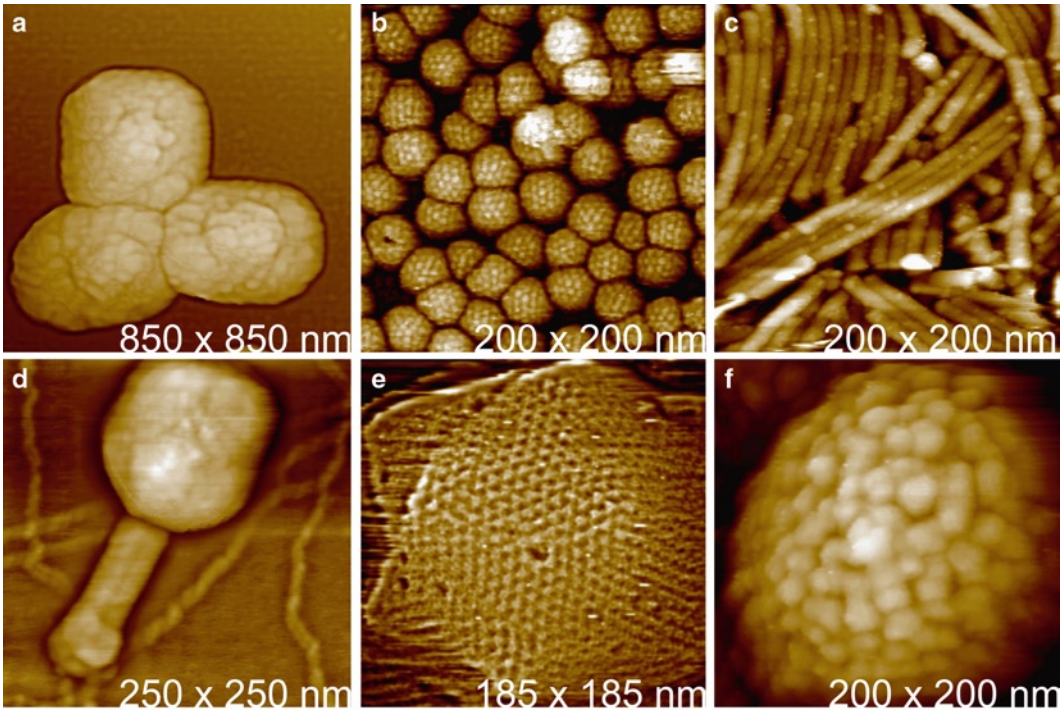


Fig. 3. A variety of viruses seen at relatively low magnifications by AFM. In (**a**) vaccinia virus, in (**b**) the retrotransposon Ty3, in (**c**) Tobacco Mosaic Virus, in (**d**) T4 bacteriophage, in (**e**) PBCV-1 algal virus, an irridovirus, and in (**f**) Moloney Mouse Leukemic Virus. The scan areas are (**a**) 850 nm × 850 nm, (**b**) 500 nm × 500 nm, (**c**) 200 nm × 200 nm, (**d**) 250 nm × 250 nm, (**e**) 185 nm × 185 nm, and (**f**) 200 nm × 200 nm.

risky to measure linear dimensions directly by AFM (see Note 3). It is, however, safe to measure the heights of objects above the substrate plane, and the distances between the points of maximum elevation (e.g., capsomere to capsomere) on particles, or center-to-center distances (e.g., particles in a crystal or in a cluster).

As has been emphasized already, for spherical and cylindrically symmetric particles, measurements of particle heights above the substrate plane yield reasonably accurate values for their diameters, and individual measurements are usually accompanied by rather modest error, generally of the order of 5% or less. By repeating measurements for a number of particles in the field, and using different scan directions, good statistics can be obtained, and histograms of size distributions compiled. Precision of a few angstroms is possible. Histograms of particle sizes, as illustrated in Fig. 4, are often informative (8, 22) (see Note 7).

### *3.6. Topography as a Function of Composition and Architecture*

The surfaces of virus particles vary topographically as a function of their composition and architectures. Plant viruses, for example, generally exhibit protein capsids with few embellishments, and this is true of many animal viruses and bacteriophages as well. These capsids are generally based on icosahedral architectures,

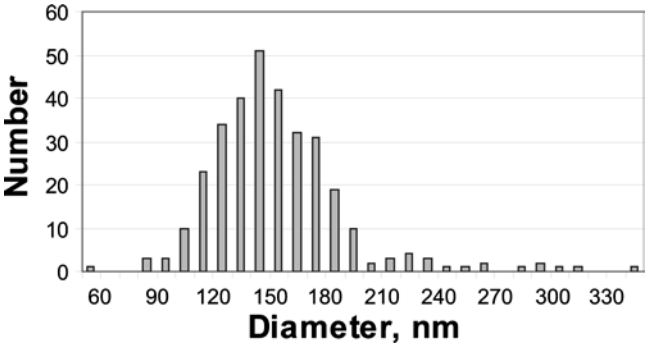


Fig. 4. The heights above substrate level were measured for about 200 isolated MuLV virions and plotted as a histogram. The spread of sizes is not due to error in the measurements, which is only a few nanometers at most, but represents the real variation in size of particles produced in infection. The very large and very small particles are aberrant virions.

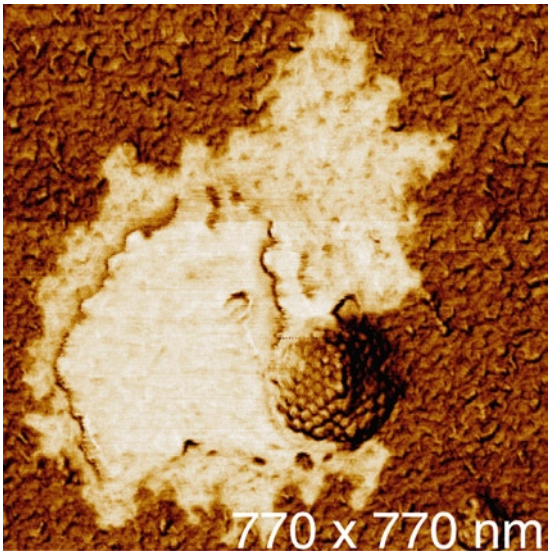


Fig. 5. A phase-contrast AFM image of a herpes simplex virion absorbed onto mica. The large sheet of *white material* around the capsid is the membrane envelope of the virus that has been partially discarded. The capsid lattice of the virus is clearly evident. The scan area is 770 nm × 770 nm.

and clusters of coat protein subunits, or capsomeres, are symmetrically distributed (28, 29). Many animal viruses, on the contrary, though they may contain an icosahedral capsid in their interior, often have either a lipid membrane over their surface, as does the herpes virus in Fig. 5, a covering of protein clusters, or even a hair-like coating of fibers. These various surfaces are readily apparent by AFM, and can be identified and delineated with a high degree of precision with the aid of some histological procedures, such as osmium tetroxide fixation, or protease treatment.

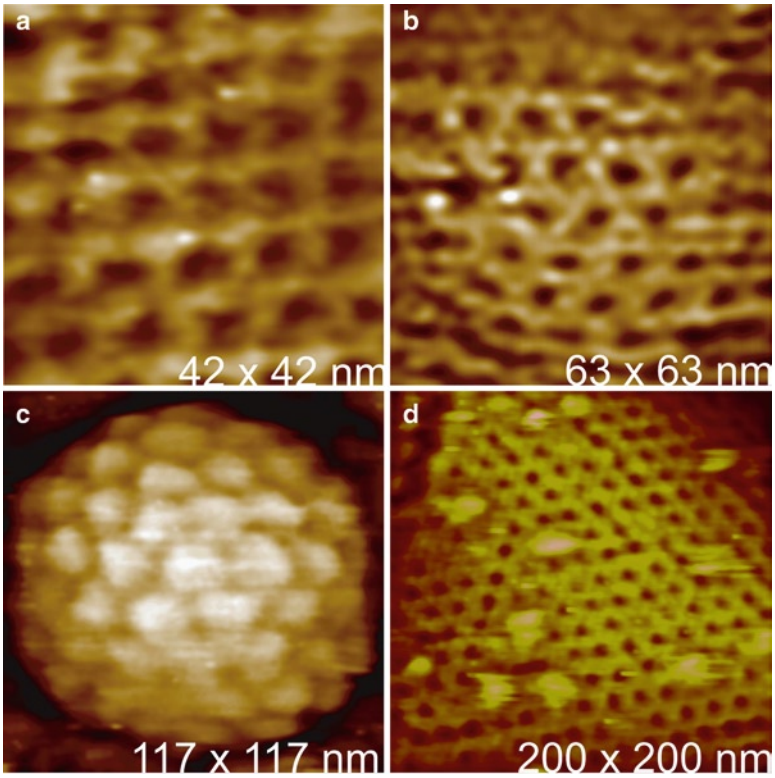


Fig. 6. At higher magnification, the surface features of many viruses emerge. Seen here in (**a**) is the surface lattice of PBCV-1, a giant algal virus belonging to the irridovirus family, in (**b**) in vitro reassembled particles of the Gag protein from Mason–Pfizer Monkey Virus, in (**c**) Ty3 retrotransposons, and in (**d**) the capsid of the giant Mimivirus. The scan areas are (**a**) 42 nm × 42 nm, (**b**) 63 nm × 63 nm, (**c**) 117 × 117 nm, and (**d**) 200 nm × 200 nm.

Icosahedral capsids, or bullet-shaped or elongated capsids based on that symmetry, can be characterized in terms of the structure of the fundamental capsomere, along with the icosahedral triangulation number, $T$ (29). Some examples are shown in Fig. 6. This will vary from small integral numbers like $T = 1$ for satellite viruses, or the $T = 1$ reassembly particles of *Brome Mosaic Virus* (30) to $T = 3$ and higher for more conventional, small icosahedral viruses such as poliovirus or TYMV, to very large numbers for complex viruses such as the irridoviruses such as PBCV-1 ($T = 169$) and mimivirus ($T$ one of nine possibilities lying between 972 and 1,200). In many cases, the exterior shell of a virus may not be icosahedral, but it might possess an inner capsid which is. For example, though membrane covered and of pleiomorphic external shape, herpes simplex virus possesses a nucleic acid containing capsid of icosahedral form $T = 16$. Mimivirus exhibits a complex outer surface coated with a forest of fibers, but it too contains an

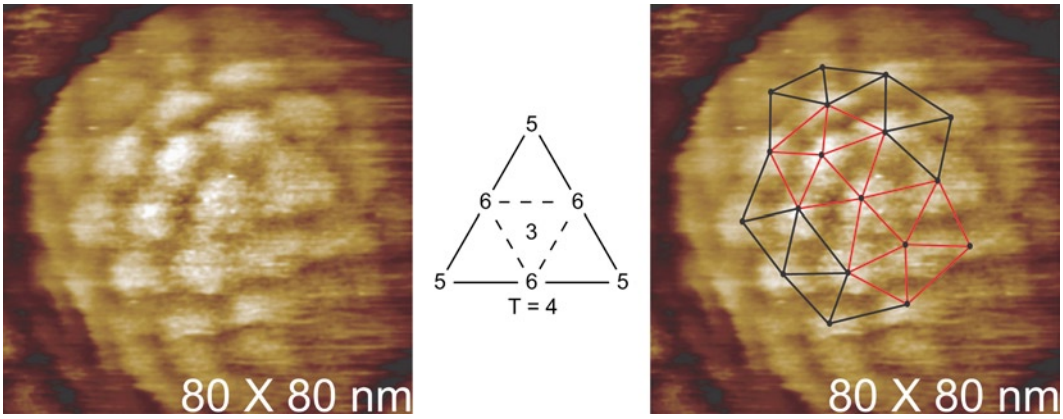


Fig. 7. On the *left* is a capsid of the Ty3 retrotransposon. If the pattern of five- and sixfold capsomeres are plotted on its surface, as on the *right*, then it can be deduced that the virion has $T = 4$ icosahedral symmetry as shown in the *center drawing*. Other Ty3 virions were shown to have $T = 3$ and $T = 7$l icosahedral architectures.

icosahedral core (9). The $T$ number, then, provides much of the information one needs to describe an icosahedral capsid.

The triangulation numbers of icosahedral viruses can frequently be deduced from AFM images, as for the retrotransposon Ty3 in Fig. 7. With very large icosahedral capsids, which include PBCV-1 and mimivirus, one determines the two indices $h$ and $k$ (29), which define $T$ ($T = h^2 + hk + k^2$). This is done by following a row of hexagonal capsomeres from one pentagonal vertex to the next icosahedral edge, and by simply counting the number of capsomeres along one edge $h$ and the other $k$ (the $h$ and $k$ coordinates of the intersection point on the icosahedral edge) that one needs to traverse (31) (see Note 8).

In the cases of Ty3 retrotransposon and of *Mason–Pfizer monkey virus* (MPMV) in Fig. 8, for example, particles of their truncated Gag proteins were reassembled in vitro and imaged at high magnification by AFM. From the images, individual protein subunits were visible, and this allowed the discrimination of two possible models for the capsomeres (5). A similar analysis was used in the case of the large algal virus PBCV-1 (8). Knowing the diameters of capsomeres is often of considerable importance, even when individual subunits cannot be resolved. In mimivirus, for example, capsomere diameter provided a crucial clue in delineating the capsid architecture and permitting subsequent detailed analysis and reconstruction by cryo-EM (9). Although capsids of native HIV have yet to be visualized by AFM, helical tubes of capsid protein reassembled in vitro have (5). In these tubes, a hexagonal arrangement of coat proteins could be clearly seen, and this provided support for a capsid model based on modified icosahedral architecture (32). The tubes reassembled from HIV Gag protein should remind us that helical and rod-shaped structures having periodic substructure are also excellent specimens

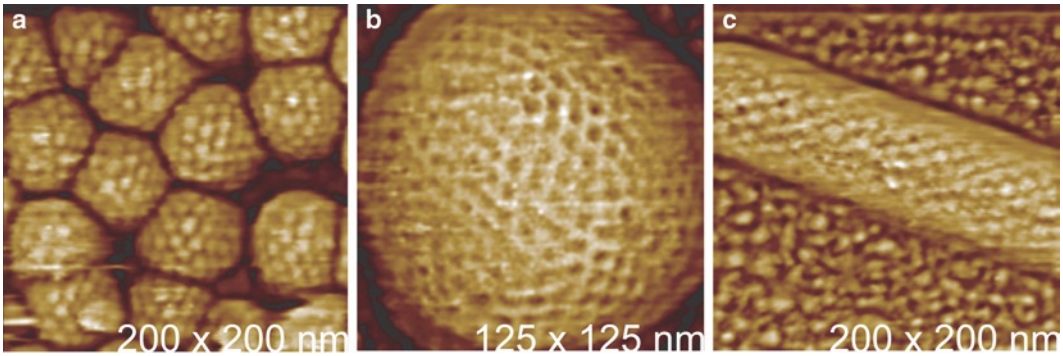


Fig. 8. Virus-like particles (VLP) reassembled in vitro or in recombinant bacteria often appear to have icosahedral symmetry, but upon closer inspection, they do not, the pentameric vertices are replaced by random defects or overall disorder. This is true of the Ty3 Gag particles in (**a**) and the mutant Gag of MPMV seen in (**b**). VLPs often take on entirely different shapes than the native capsids, as seen in the *tubular forms* of reassembled HIV Gag in (**c**). The scan areas are (**a**) 250 nm × 250 nm, (**b**) 125 nm × 125 nm, and (**c**) 200 nm × 200 nm.

for AFM analysis. These can appear in investigations of intact viruses and even in studies of spherical viruses when their interiors are explored.

### 3.7. Virus Sample Preparation Techniques

#### 3.7.1. Isolated Particles

With AFM, it is not essential that highly purified virus particles be used as samples (15), although that might be ideal. Because individual particles can be investigated whenever a good specimen is spatially distinct from the surrounding rubble of proteins, cellular debris, and biological detritus, it may still yield excellent images. A problem, however, is that biological debris often adhere to and foul the AFM tip, severely degrading the quality of images. Contaminated tips are one of the most frustrating and annoying accompaniments of biological AFM.

#### 3.7.2. Viruses on the Surface of Host Cells

Viruses on the surfaces of host cells may be visualized as well as free particles, and sometimes with better results because they are better immobilized (8, 20, 22, 33). *Moloney mouse leukemia virus* (MuLV) emerging from an infected 3T3 cell are clearly delineated in Fig. 9. They may be seen entering cells upon infection, or budding from cells after replication and assembly. This often provides valuable insights into which cells in a population are producing virus, the distribution of virus particles on the surface of the cells (are there preferred sites for budding?), and some details of the budding process itself.

#### 3.7.3. Mutant Viruses: Anomalous Features

Mutant viruses, naturally occurring or produced in the laboratory, can be imaged as well as native virions and virus-like particles (VLP) created in vitro from capsid proteins. In some cases, the phenotype of the mutant can be revealed by observing infected host cells for unique or anomalous features. This was done, as shown in Fig. 10, in a study of MuLV-infected 3T3 cells, where a

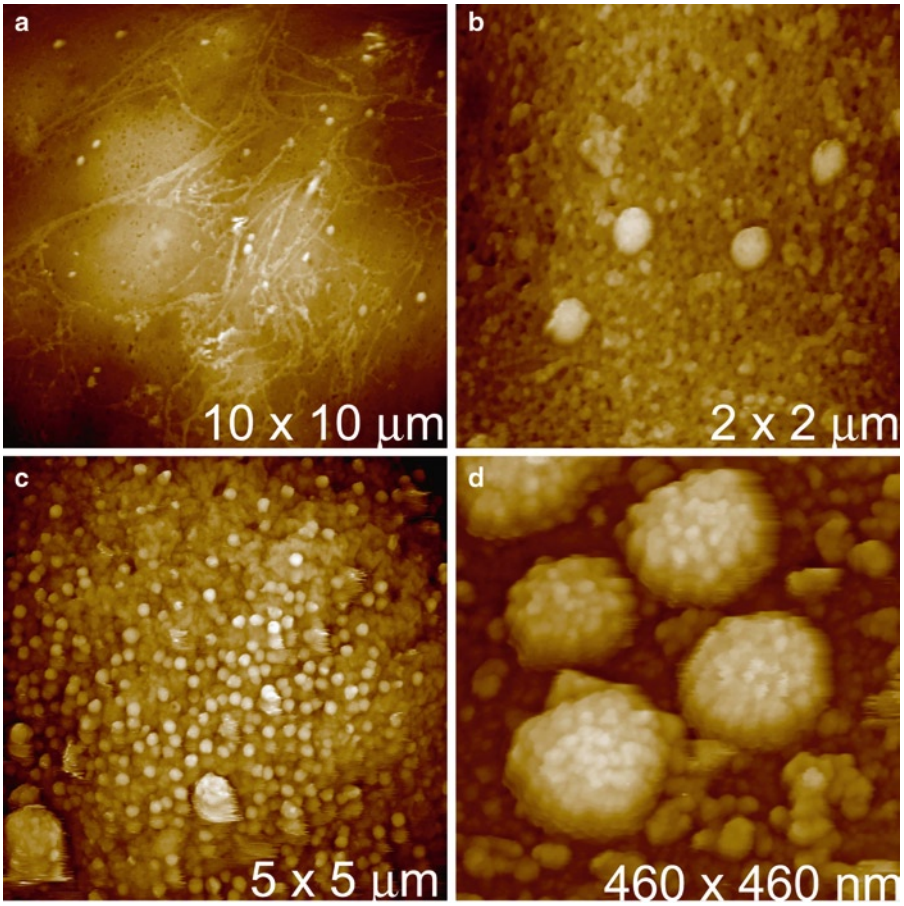


Fig. 9. Viruses can also be observed while emerging from, or stall attached to the host cell plasma membrane. In (**a**) is a low magnification AFM image of a 3T3 cell in culture infected with MuLV. The virus is clearly seen as *white spots* over the surface of the cell. In (**b**) is a higher magnification image showing four MuLV particles budding from a host cell in culture. In (**c**) is a mass of HIV virus bursting from the surface of a human lymphocyte in culture, and in (**d**), a higher magnification image of four HIV budding from a lymphocyte surface. The scan areas are (**a**) 10 µm × 10 µm, (**b**) 2 µm × 2 µm, (**c**) 5 µm × 5 µm, and (**d**) 460 nm × 460 nm.

mutant lacked glycosylated Gag protein (20, 34). Prior evidence suggested that such mutants failed in some stage of viral budding. This was confirmed by AFM visualization of infected, virus-producing cells. As seen in Fig. 10, instead of normal, spherical virus emerging from the cell surface, bullet- and comet-shaped protrusions were found distributed all over the plasma membrane of the host cells. The comets were viruses that were apparently trying to escape, but were unable to pull away and terminate association with the host cell. From this, it was concluded that the failure of glycosylation produced a defect in late stages of the budding process.

Other mutations in virus genomes may produce alterations in external features of virus particles that are readily observable by AFM.

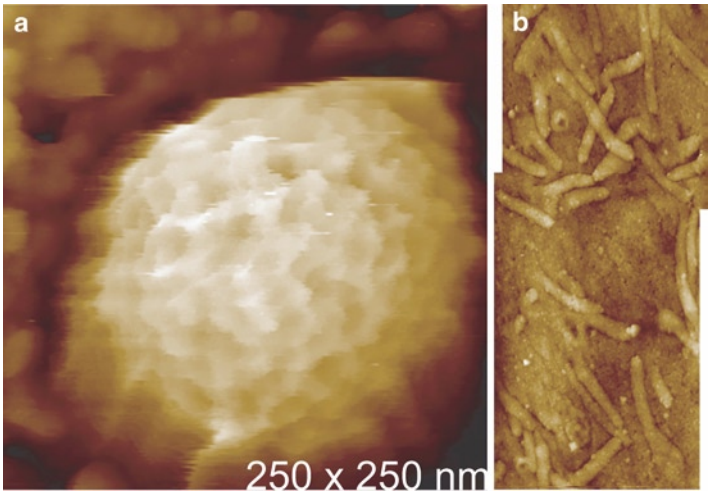


Fig. 10. Two mutant forms of Moloney Mouse Leukemic Virus (MuLV) are shown in (**a**) and (**b**). In (**a**), the mutant lacks the ability to make the envelope protein, and the lipid membrane of the virus is observed directly. Its *wavy pattern* is due to its fluid nature and its motion when subjected to the pressure of the AFM cantilever. In (**b**) is another mutant which does not properly glycosylate its Gag protein, resulting in an inability to bud from the host cell properly, resulting in the *comet-shaped structures* on the surface of the host 3T3 cell in culture. The scan areas are (**a**) 250 nm × 250 nm. In (**b**) are composites of serial, positionally incremented AFM images representing total scan areas of 2 μm × 8.44 μm and 2 μm × 4.72 μm.

MuLV particles that failed to make an envelope protein (gp120 protein), one of which is seen in Fig. 10, were examined in another study (22). While normal particles are characterized by a coating of protein tufts, about 100–150 in number, mutant particles were "bald" virions lacking any such protein clusters. Instead, only an outer lipid membrane was visible.

Some viruses exhibit special external structures, or deviations from their general architectures. For example, MuLV particles generally have a single small bump or a brief protrusion somewhere on their otherwise uniformly crenulated surfaces. These are likely to be a "budding scar" resulting from breaking away from the host cell (22). Other MuLV particles, perhaps defectives, exhibited small sectors on their surfaces where protein was absent and a channel into the interior appeared (20). Other, more prominent features are the surface fibers on the surfaces of mimivirus and the lateral bodies of vaccinia (seen in Fig. 11) (25, 26).

PBCV-1 *Chlorella Virus*, an irridovirus, exhibited a unique pentagonal assembly of proteins at every fivefold vertex of its icosahedral capsid (8), shown in Fig. 12. The assembly had a single protein in the center that could "push in" and "pull out" as demonstrated by the application of AFM tip pressure. Its exact function is speculative. Many bacteriophages have tail assemblies of one sort or

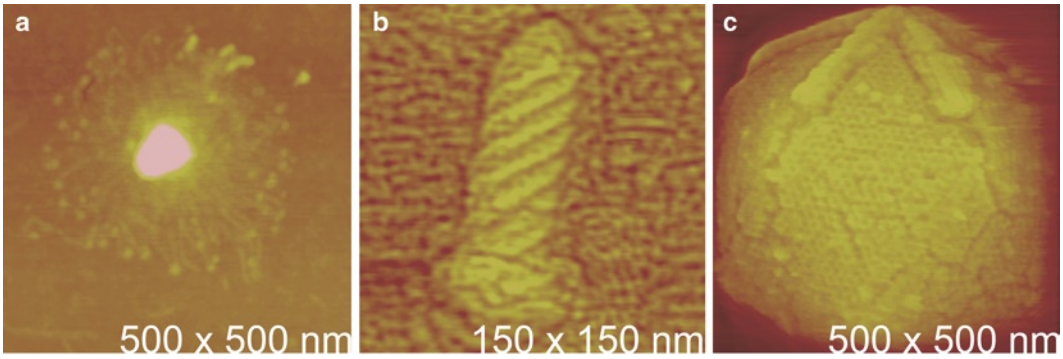


Fig. 11. AFM can capture a variety of specialized structures produced by viruses. In (**a**) is a fragment of the anchor protein, at the *center*, which connects a corona of glycosylated surface fibers to the capsid. In (**b**) is the contractile DNA injection assembly, or tail, of bacteriophage T4 showing helical architecture. In (**c**) is the "stargate" apparatus found at a unique vertex of Mimivirus which, upon opening, allows escape of the DNA.

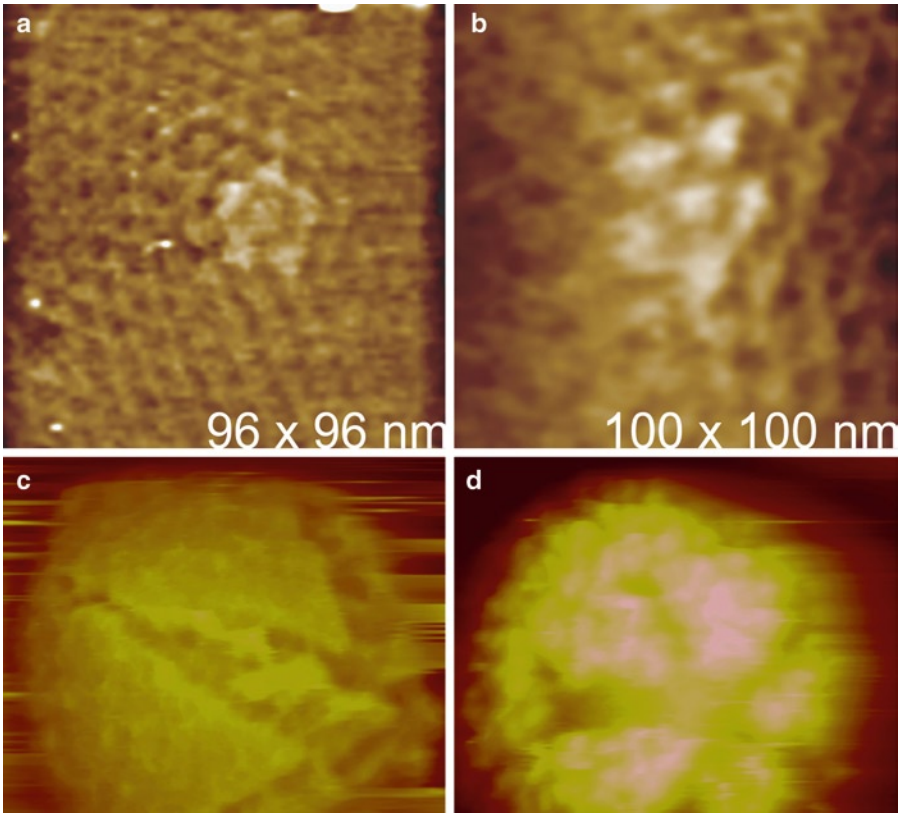


Fig. 12. Fivefold vertices on large viruses which have icosahedral capsids often have unique clusters of proteins or unusual structures. In (**a**) and (**b**) are fivefold vertices of the large algal virus PBCV-1. In (**c**) and (**d**) is seen the stargate apparatus of Mimivirus opening to allow expulsion of the DNA inside the capsid. The scan areas are (**a**) 96 nm × 96 nm, (**b**) 100 nm × 100 nm, (**c**) 500 nm × 500 nm, and (**d**) 800 nm × 800 nm.

another for packaging and injecting their DNA. Mimivirus is, in a sense, similar to these phages and has an assembly, seen in Fig. 12c, d, of presumably similar function at a single, unique, fivefold vertex. This star shaped structure is undoubtedly analogous to the tail assemblies of phages and is, as is evident in the figures, a distinctive feature of the virions. It is a complex structure likely composed of many proteins, and AFM reveals much of that complexity.

### 3.8. Population Analysis

An important point that deserves particular emphasis is that all of the particles within a population of virus are not absolutely identical, and often there are very significant differences in the detailed features of individual virus particles. This is a point often obscured by the results of X-ray crystallography (35, 36) or cryo-EM reconstructions (37, 38). These techniques rely totally on an assumption of structural conformity and produce models that represent the average in time and space of the individuals that make up the population. AFM, on the contrary, allows the revelation of the eccentricities and unique features of the individuals, and these are instructive. They often define the extremes of what is possible among a large population of viruses having, presumably, the same genome and the same environment for replication and assembly. What we see with AFM is that anomalous and aberrant individuals are not only present, but are also common.

### 3.9. Internal Structure Determination

One might think that because AFM provides images of the surfaces of objects and does not peer into their interiors, as do X-ray diffraction and electron microscopy, they would be of little value in delineating the interior structure of viruses, the layers beneath the external surface. This is not true, however, as we can apply the same technique that has been used by anatomists for centuries – dissection. With the aid of chemical, enzymatic, and physical tools, we can systematically pare a complex entity, including a virus, down to its core, layer by layer (23). At each stage, AFM may then be used to visualize what remains and what has been removed as well (see Note 9).

Among the most useful agents for chemical dissection have been detergents, usually 0.5–2% of some nonionic detergents such as NP40, and reducing agents such as DTT or DTE. The former causes protein structure to unravel gradually and detergents strip away the lipid membrane. The latter reduces disulfide bonds and liberates polypeptides otherwise bonded to one another. Disulfide bond reduction appears to be particularly important in large, complex viruses where such covalent linkages cross-link coat proteins and stabilize capsids (25, 39) (see Note 10).

The most effective enzymatic tools have been proteases that degrade polypeptides. These are particularly useful because they have a range of activities and a spectrum of specificities. As a consequence, a whole variety of proteases have been employed, including trypsin, bromelin, proteinase K, subtilisin, and mixtures

of pancreatic proteases. Viruses are usually exposed to the proteases for anywhere from 15 min to several hours, or even overnight, at concentrations of 0.5 mg/ml to as high as 5 mg/ml (see Note 11).

Physical forces have also been used to disrupt viruses, and often fortuitous perturbations, resulting simply from preparation and handling, have proven to be structurally illuminating. Heat, for example, was used to open TYMV (7) to release its encapsidated RNA, and direct physical pressure was used on mimivirus sandwiched between two layers of atomically smooth cleaved mica, as well. There are also instances where "hammering" of individual particles with the AFM tip has been utilized, taking advantage of the fact that AFM can serve as a tool as well as an imaging device.

In carrying out the dissection of a virus, or even in simply visualizing particles spread on a glass, plastic, or mica substrate, it is necessary to ensure that the virus particles adhere firmly to the substrate. Failure to do so allows the particles to move beneath the AFM tip, rendering imaging impossible. Occasionally, altering the charge on the substrate is sufficient (see Notes 12 and 13).

Altering charge is, however, frequently insufficient for virions. To fix most viruses to the substrate, as well as a wide variety of other biological entities and materials, an effective procedure is to coat the substrate with poly-L-lysine before depositing the virus. Presumably, salt bridges between the ε amino groups of the lysines and the glutamic and aspartic acid carboxyl groups on the particles lock them in place. After such substrate–particle attachment, the substrate can be rinsed with water several times without loss of sample (see Note 14).

It is occasionally unnecessary to actually treat viruses with any chemical or biochemical agent to view the interior, as the physical stress of preparation and purification may result in damaged or partially degraded particles. These may expose interior structural features that are otherwise not apparent. Retroviruses, in particular, are physically fragile. Some MuLV, as shown in Fig. 13, when subjected to the shear forces of centrifugation, lose portions of the shell surrounding the capsid. This permits direct visualization of the virus core still embedded within the layers of envelope and matrix protein (22).

HIV is another example where even the mildest procedures produce some damaged virions. Although the cores of HIV have not yet been visualized by AFM, likely due to their fragility, the remainder of the virus without the cores has been (22). Some examples can be seen in Fig. 13c, d. Such partially disrobed particles, both MuLV and HIV, provide specimens that can be subjected to quantitative examination and thereby yield the dimensions, the thicknesses of internal structural layers, and they give some clues as to their components as well.

The best example of a complete dissection of a complex virus using AFM is that of vaccinia virus, a pox virus of about 300-nm

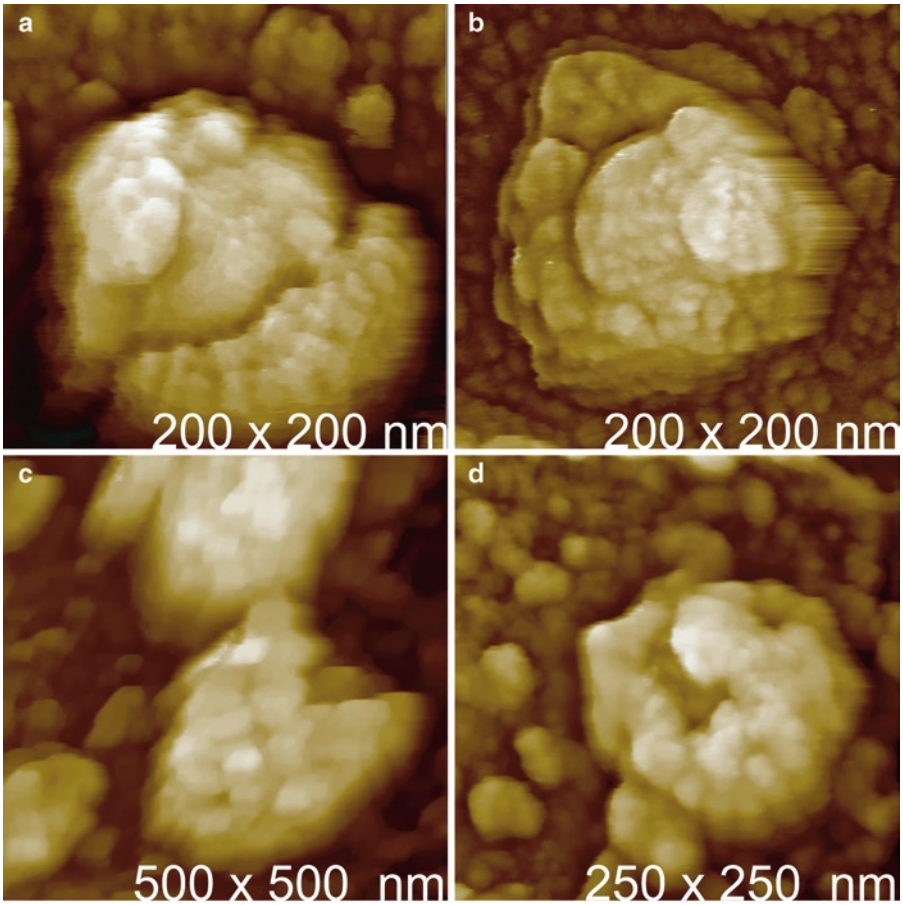


Fig. 13. Virions are sometimes damaged in their preparation, especially fragile viruses such as retroviruses. These occasions often provide images of interior structure that would otherwise not be accessible to the AFM tip. In (**a**) and (**b**) are MuLV whose outer shell has been partially sheared away to reveal the nucleic acid containing capsid inside. In (**c**) and (**d**) are similarly sheared HIV particles. The interior capsids have been lost, leaving the empty outer shells behind. The scan areas are (**a**) 200 nm × 200 nm, (**b**) 200 nm × 200 nm, (**c**) 500 nm × 500 nm, and (**d**) 250 nm × 250 nm.

diameter that is delimited by a lipid membrane (25, 26). It contains a double-stranded DNA genome bounded by several protein shells. It also has two unusual protein assemblies of still unknown function, known as lateral bodies, associated with its inner core. Vaccinia was sequentially degraded with a 0.5% NP40 nonionic detergent combined with 0.05 M DTT, followed by exposure to this same mixture but containing either trypsin or proteinase K, or to the proteases alone. Six stages in this process are presented in Fig. 14. At the end, the innermost core was breached and the DNA was exposed.

### *3.10. Imaging of Nucleic Acids of Viruses*

The nucleic acids of viruses, some of which are seen in Fig. 15, from a structural standpoint, are of considerable interest, and in particular, how they are condensed and packaged inside capsids and cores. Clearly, packaging is accomplished differently by specific families of viruses. It is unlikely, for example, that

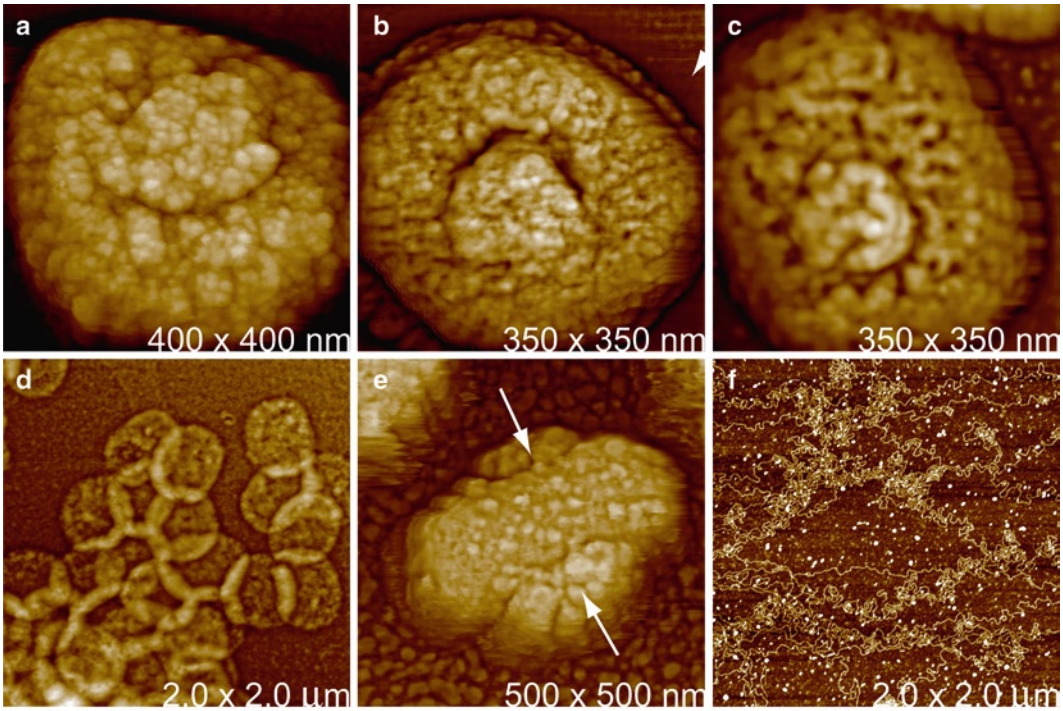


Fig. 14. A series of AFM images presenting the dissection of vaccinia virus using a variety of enzymatic and chemical reagents to remove successive layers of structure. In (**a**) is the intact virus in buffer before any treatment. In (**b**), the lipid membrane is pronounced as a corona surrounding a virion dried upon the substrate. The lateral body at the *center* is also more pronounced on the dried virions. In (**c**), the outer protein shell has been etched away to reveal the inner protein capsid which is perforated and still has the lateral bodies connected to it. In (**d**) is a mass of capsids having lost both their lateral bodies and their DNA. In (**e**) are higher magnification AFM images of the lateral bodies that decorate the capsids, and in (**f**) is a mass of vaccinia DNA released onto the AFM substrate. The scan areas are (**a**) 400 nm × 400 nm, (**b**) 350 nm × 350 nm, (**c**) 350 nm × 350 nm, (**d**) 2 µm × 2µm, (**e**) 500 nm × 500 nm, and (**f**) 2 µm × 2 µm.

bacteriophage and pox virus package their genomic double-stranded DNA the same way. The packing densities of the nucleic acid differ by more than tenfold (26). Also, is it unlikely that large, single-stranded RNA-containing viruses, such as retroviruses, package their genomes the same way as do $T=1$ or $T=3$ icosahedral viruses (40). Certainly, helical and filamentous viruses use entirely different mechanisms.

AFM investigations have been conducted on RNA extracted by phenol from a series of small icosahedral viruses, and from tobacco mosaic virus, the classical rod-shaped, helical virus (41). The spherical viruses included poliovirus, STMV, TYMV, and brome mosaic virus. In this study, the gradual unraveling of the tertiary structure of the RNA, and ultimately the secondary structure as well, could be produced in stages simply by heating. A counter example was provided by the rod-shaped, helical tobacco mosaic virus RNA which appeared initially as a thread, a completely extended molecule lacking any secondary structure. With time, it began forming local secondary structural elements

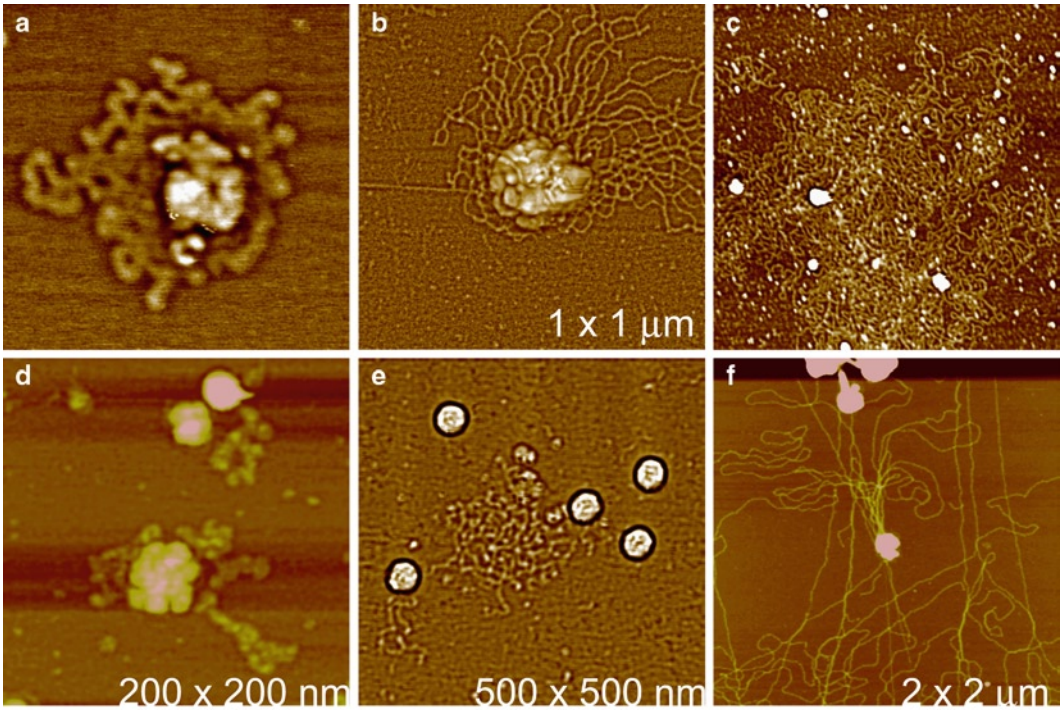


Fig. 15. Expulsions or emissions of nucleic acid by a variety of viruses. In (**a**), a shattered Ty3 retrotransposon disgorges a mass of nucleic acid. Although it is known that the genome of the retrotransposon has two single strands of RNA as its genome, the nucleic acid seen here has the characteristics of double-stranded DNA. In (**b**), the DNA core of the algal virus PBCV-1 throws out a splash of double-stranded DNA. In (**c**) is a mass of DNA released by vaccinia virus upon degradation with proteases. In (**d**), a shattered virion of STMV spreads its single-stranded RNA genome of 1,058 nucleotides around itself. In (**e**), virions of TYMV are losing their single-stranded RNA genomes after loss of a capsomere. In (**f**), damaged T4 bacteriophages release their DNA on the AFM substrate. The scan areas are (**a**) and (**b**) 1 µm × 1 µm, (**c**) 5 µm × 5 µm, (**d**) 200 nm × 200 nm, (**e**) 500 nm × 500 nm, and (**f**) 2 µm × 2 µm.

and eventually condensed into forms similar to those seen for the RNA from the icosahedral viruses (41). One conclusion of the study was that the single strands of RNA spontaneously condensed as linear arrangements of stem-loop substructures following synthesis, the condensed RNA bound coat protein to it, and the two cooperatively coalesced into the completed particle. In studies such as these, AFM proved itself as an able technique for directly visualizing nucleic acid structure, demonstrating its fluidity, and suggesting the mechanisms by which it is encapsidated.

DNA and RNA appear quite different in AFM images, and this is evident in Fig. 16, which presents both kinds of nucleic acids. The former looks like strands and coils of stiff rope lacking any higher levels of structure, while the latter appears as complicated, linear sequences of self-involved secondary structure. Sometimes, however, the distinction is not entirely clear and further evidence may be needed to show whether a filament, strand, or complex is DNA or RNA.

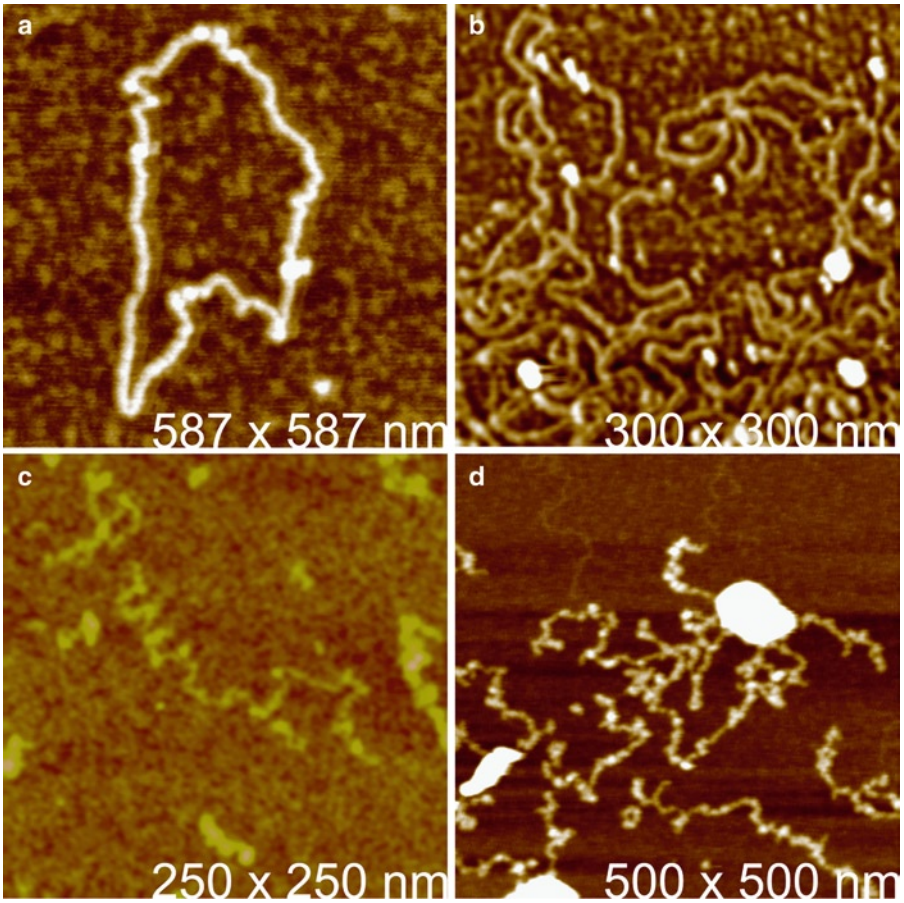


Fig. 16. Viral nucleic acid can be readily visualized by AFM after expulsion from the capsid. In (**a**) is a DNA plasmid used in recombinant DNA research to transform bacteria. In (**b**) is a tangle of double-stranded DNA from vaccinia virus. In (**c**) is the genomic single-stranded RNA of STMV, still condensed due to secondary structure, and in (**d**), RNA from poliovirus escaping from a condensed core obtained by phenol extraction of the virus. The scan areas are (**a**) 587 nm × 587 nm, (**b**) 500 nm × 500 nm, (**c**) 220 nm × 220 nm, and (**d**) 500 nm × 500 nm.

A method was devised for additional identification based on exposure of the nucleic acid to high concentrations of bovine RNase A (42). RNA, naturally, was hydrolyzed to small pieces by RNase A and left only fragments on the substrate which corresponded to protected stem-loops. DNA, on the contrary, became coated with the protein and the resulting strands exhibited diameters two to three times that of naked double-stranded DNA. Thus it is possible to practice a kind of crude histology with AFM.

A second example of histological AFM is the immunolabeling of viruses with antibodies specific for certain proteins. Although individual IgG are not clearly identifiable by AFM when bound to a virion, IgG conjugated with gold particles generally are. In a sense, these are used in the same way as they are used in transmission electron microscopy immunolabeling, except that instead of visualizing points of high electron density, one images with AFM objects having the size and shape of the immuno-gold particles.

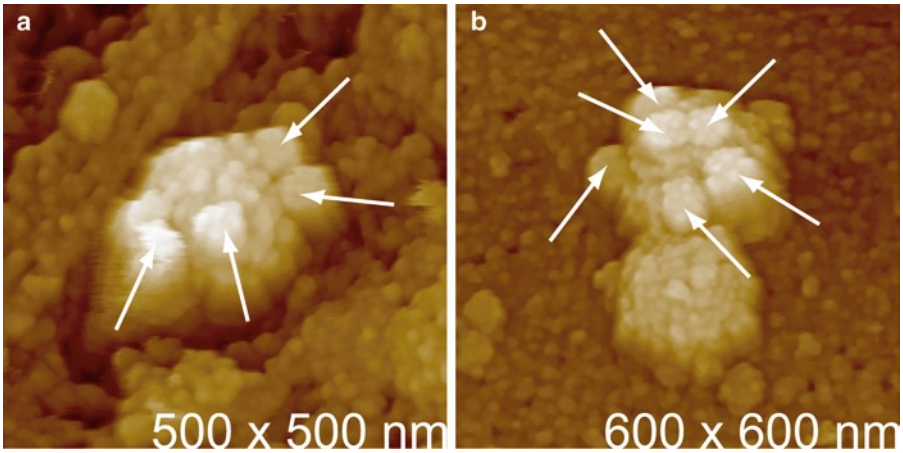


Fig. 17. Virus can be labeled with gold particles conjugated with antibody against specific viral proteins. These can be visualized using AFM as seen here. In (**a**) and (**b**) are two different MuLV virions that have been exposed to antibody/gold particles directed against the envelope protein. *Arrows* indicate the gold particles. The scan areas are (**a**) 500 nm × 500 nm and (**b**) 600 nm × 600 nm.

Using gold–IgG conjugate particles against the envelope protein, as shown in Fig. 17, it was possible to show that protein tufts on the surfaces of MuLV were indeed envelope proteins (20, 22). The major problem with IgG–gold conjugates at this point is that their physical size limits the resolution of the method. Conjugated gold particles can bind only as close as their diameters allow.

The answer to the question, what can AFM visualize that is of value to the structural biology of viruses, is that it can visualize virtually every part of a virus, and to resolutions that approach, and in some cases surpass, those of electron microscopy. At this time, lipid membranes have been identified, both RNA and DNA have been visualized, and large protein assemblies resolved. The capsids of icosahedral viruses, and the icosahedral capsids of non-icosahedral viruses have been seen at high resolution, in some cases sufficiently high to deduce the arrangement of coat protein units in the capsomeres, or to determine the triangulation number *T*. In addition, viruses have been recorded budding from infected cells and suffering the consequences of a variety of stresses. Mutant viruses have been examined and phenotypes described. Unusual structural features have appeared, and very importantly, the unexpectedly great amount of structural non-conformity within populations of virus particles has been well documented. It has, furthermore, been shown that the structures of viruses observed by AFM are entirely consistent with models derived by X-ray crystallography and cryo-EM (16). Although there are currently no examples, there is certainly no reason why structural information derived from X-ray crystallography and/or electron microscopy cannot be combined with AFM images, just as it has been for the latter two technologies.

## 4. Notes

1. Tapping mode minimizes contact between the probe tip and the sample surface and greatly reduces lateral forces. An even more sensitive means of scanning in tapping mode is called phase modulation scanning. Here, phase changes are introduced into the tip oscillations due not only to height differences, but also to changes in the nature of the aggregate atomic interactions, caused in turn by variations in the physical or chemical properties of the sample surface. This approach has been shown to be useful for imaging very thin and delicate materials such as biological membranes (24).
2. To achieve this, it may be necessary to treat the substrate with various reagents, such as poly-l-lysine, to induce better adhesion of samples. If this condition is not met, then the specimen will move due to interaction with the probe, and no useful information will be gathered.
3. Because one does not, in general, know the tip shape one is working with at the time, the image cannot be easily deconvoluted to provide true lateral dimensions.
4. On large soft samples, such as living animal cells (33), lateral resolution may be more limited by the motion and deformation of the cell surface in response to tip pressure rather than tip structure.
5. Because visualization can be carried out in a fluid environment, specimens may suffer no dehydration as is generally the case with electron microscopy, and they usually require no fixing or staining.
6. Indeed, specimens can be observed over long periods, so long as they stay relatively unchanged and immobilized during a single frame interval. For the most part, even living cells seem oblivious to the presence of the probe tip (33).
7. If the distribution is a simple Gaussian, then it can be presumed that particles of only one general morphology, or icosahedra of only one triangulation number are present, but that their diameters vary to some degree about the mean, perhaps due to physiological state or degree of maturation. On the contrary, if a more complex distribution is observed, one having multiple peaks and shoulders, then particles of separate classes may be present.
8. While the *T* number describes the overall distribution of capsomeres on the surface of an icosahedral capsid, the more complete description of a virus structure would require the distribution of protein units in the individual capsomeres to be defined, and ultimately coordinates of the atoms

comprising the virus coat proteins. The last can only be obtained by X-ray crystallography, but the distribution of subunits within capsomeres can sometimes be determined or deduced by AFM analysis.

9. This approach is particularly effective with large, complex viruses such as vaccinia virus (25, 26) or mimivirus (9). With these large assemblies, ordered and disordered protein shells, lipid membranes, and the nucleic acid within can be revealed and analyzed. By deconstruction, the architecture of particles is revealed, and, at the same time, the kinds of biochemical interactions that maintain each level of structure are delineated as well.
10. In some cases, nonionic detergents are insufficient to disrupt structure and more vigorous ionic detergents such as SDS must be used. There is difficulty with SDS, however. It tends to have an all-or-none effect, so that upon reaching a concentration sufficient to disrupt viruses, it completely degrades them uncontrollably. SDS can also produce artifacts due to drying on the substrate.
11. The proteases must be washed from the virions with buffer or water before imaging as they otherwise produce a dense, irregular background that makes imaging problematic, and they foul the cantilever tip.
12. Mica is negatively charged on its surface, but exposure to nickel or magnesium salt such as $MgCl_2$ coats it with divalent ions and leaves it positively charged.
13. Some viruses or macromolecules, such as nucleic acids, may be firmly held by a positive surface if they are repelled by a negative surface, or vice versa.
14. The only serious disadvantage of coating with poly-l-lysine is that it produces a rather rough and irregular background. As a consequence, molecular objects, such as lipid membranes or nucleic acids, which rise only about a nanometer or two above the substrate plane, become difficult to identify and visualize. The method is excellent, however, for imaging cells and intact or partially degraded virions.

## References


1. Binning, G., and Quate, C.F. (1986). Atomic force microscope. *Phys. Rev. Lett.* **56:** 930–933.
2. Bustamante, C., and Keller, D. (1995). Scanning force microscopy in biology. *Phys. Today* **48**: 32–38.
3. Allen, S., Davies, M.C., Roberts, C.J., Tendler, S.J.B., and Williams, P.M. (1997). Atomic force microscopy in analytical biotechnology. *Trends in Biotech.* **15**: 101–105.
4. Hansma, P.K. (1994). Tapping mode atomic force microscopy in liquids. *Appl. Phys. Lett.* **64**: 1738–1740.
5. Kuznetsov, Y.G., Ulbrich, P., Haubova, S., Ruml, T., and McPherson, A. (2007).

Atomic force microscopy investigation of Mason-Pfizer monkey virus and human immunodeficiency virus type 1 reassembled particles. *Virology* **360**: 434–446.

6. Baker, T.S., Olson, N.H., and Fuller, S.D. (1999). Adding the third dimension to virus life cycles: Three-dimensional reconstruction of icosahedral viruses from cryo-electron micrographs. *Microbiology and Molecular Biology Reviews* **63**: 862–922.
7. Kuznetsov, Y.G., and McPherson, A. (2006). Atomic force microscopy investigation of Turnip Yellow Mosaic Virus capsid disruption and RNA extrusion. *Virology* **352**: 329–337.
8. Kuznetsov, Y.G., Gurnon, J.R., Van Etten, J.L., and McPherson, A. (2005). Atomic force microscopy investigation of a chlorella virus, PBCV-1. *J Struct Biol* **149**: 256–263.
9. Xiao, C., Kuznetsov, Y.G., Sun, S., Hafenstein, S.L., Kostyuchenko, V.A., Chipman, P.R., Suzan-Monti, M., Raoult, D., McPherson, A., and Rossmann, M.G. (2009). Structural studies of the giant mimivirus. *PLoS Biology* 7: 958–966.
10. Malkin, A.J., Land, T.A., Kuznetsov, Y.G., McPherson, A., and DeYoreo, J.J. (1995). Investigation of virus crystal growth mechanisms by in situ atomic force microscopy. *Physical Review Letters* **75**: 2778–2781.
11. Land, T.A., Malkin, A.J., Kuznetsov, Y.G., McPherson, A., and DeYoreo, J.J. (1996). Mechanisms of protein and virus crystal growth: An atomic force microscopy study of Canavalin and STMV crystallization. *J. Cryst. Growth* **166**: 893–899.
12. Malkin, A.J., Kuznetsov, Y.G., Lucas, R.W., and McPherson, A. (1999). Surface processes in the crystallization of turnip yellow mosaic virus visualized by atomic force microscopy. *J Struct Biol* **127**: 35–43.
13. Malkin, A.J., Kuznetsov, Y.G., and McPherson, A. (2001). Viral Capsomere Structure, Surface processes and growth kinetics in the crystallization of macromolecular crystals visualized by in situ atomic force microscopy. *J. Cryst. Growth* **232**: 173–183.
14. Malkin, A.J., Plomp, M., and McPherson, A. (2002). Application of atomic force microscopy to studies of surface processes in virus crystallization and structural biology. *Acta crystallographica* **58**: 1617–1621.
15. Kuznetsov, Y.G., Malkin, A.J., Lucas, R.W., Plomp, M., and McPherson, A. (2001). Imaging of viruses by atomic force microscopy. *The Journal of general virology* **82**: 2025–2034.
16. McPherson, A., Malkin, A.J., Kuznetsov, Y.G., and Plomp, M. (2001). Atomic force microscopy applications in macromolecular crystallography. *Acta Cryst.* D**57**: 1053–1060.
17. McPherson, A., Kuznetsov, Y.G., Malkin, A.J., and Plomp, M. (2004). Macromolecular crystal growth investigations using atomic force microscopy. *Journal of synchrotron radiation* **11**: 21–23.
18. Makino, D.L., Larson, S.B., and McPherson, A. (2005). Preliminary analysis of crystals of panicum mosaic virus (PMV) by X-ray diffraction and atomic force microscopy. *Acta crystallographica* **61**: 173–179.
19. Kuznetsov, Y.G., Daijogo, S., Zhou, J., Semler, B.L., and McPherson, A. (2005b). Atomic force microscopy analysis of icosahedral virus RNA. *J Mol Biol* **347**: 41–52.
20. Kuznetsov, Y.G., Datta, S., Kothari, N.H., Greenwood, A., Fan, H., and McPherson, A. (2002). Atomic force microscopy investigation of fibroblasts infected with wild-type and mutant murine leukemia virus (MuLV). *Biophys J* **83**: 3665–3674.
21. Kuznetsov, Y.G., Victoria, J.G., Robinson, W.E., Jr., and McPherson, A. (2003). Atomic force microscopy investigation of human immunodeficiency virus (HIV) and HIV-infected lymphocytes. *J Virol* 77: 11896–11909.
22. Kuznetsov, Y.G., Low, A., Fan, H., and McPherson, A. (2004). Atomic force microscopy investigation of wild-type Moloney murine leukemia virus particles and virus particles lacking the envelope protein. *Virology* **323**: 189–196.
23. Malkin, A.J., Plomp, M., Leighton, T.J., McPherson, A., and Wheeler, K.E. (2006). Unraveling the Architecture and Structural Dynamics of Pathogens by High Resolution In vitro Atomic Force Microscopy. In *Microscopy and Microanalysis*, pp. 32–85. Cambridge Univ. Press, Cambridge.
24. Plomp, M., Rice, M.K., Wagner, E.K., McPherson, A., and Malkin, A.J. (2002). Rapid visualization at high resolution of pathogens by atomic force microscopy: structural studies of herpes simplex virus-1. *Am J Pathol* **160**: 1959–1966.
25. Malkin, A.J., McPherson, A., and Gershon, P.D. (2003). Structure of intracellular mature vaccinia virus visualized by in situ AFM. *J. Viol.* 77: 6332–6340.
26. Kuznetsov, Y., Gershon, P.D., and McPherson, A. (2008). Atomic Force Microscopy Investigation of Vaccinia Virus Structure. *Journal of Virology* **85**: 7551–7566.
27. Kaper, J.M. (1975). The Chemical Basis of Virus Structure, Dissociation and Reassembly. In *The Frontiers of Biology Series.*

(eds. A. Neuberger, and E.L. Tatum). North-Holland, Amsterdam.

28. Horne, R.W., and Wildy, P. (1961). Symmetry in virus architecture. *Virology* **15**: 348–373.
29. Caspar, D.L.D., and Klug, A. (1962). Physical principles in the construction of regular viruses. In *Cold Spring Harbor Symposium on Quant. Biol.*, pp. 1–24.
30. Lucas, R.W., Kuznetsov, Y.G., Larson, S.B., and McPherson, A. (2001). Crystallization of Brome Mosaic Virus (BMV) and T = 1 Brome Mosaic Virus Particles following a structural transition. *Virology* **286**: 290–303
31. Reddy, V.S., Natarajan, P., Okerberg, B., Li, K., Damodaran, K.V., Morton, R.T., Brooks, C.L.I., and Johnson, J.E. (2001). Virus Particle Explorer (VIPER), a website for virus capsid structures and their computational analyses. *J. Virol.* **75**: 11943–11947.
32. Ganser, B.K., Li, S., Klishko, V.Y., Finch, J.T., and Sundquist, W.I. (1999). Assembly and analysis of conical models for the HIV-1 core. *Science* **283**: 80–82.
33. Kuznetsov, Y.G., Malkin, A.J., and McPherson, A. (1997). Atomic force microscopy studies of living cells: visualization of motility, division, aggregation, transformation, and apoptosis. *J Struct Biol* **120**: 180–191.
34. Low, A., Datta, S., Kuznetsov, Y., Jahid, S., Kothari, N., McPherson, A., and Fan, H. (2007). Mutation in the glycosylated gag protein of murine leukemia virus results in reduced in vivo infectivity and a novel defect in viral budding or release. *J Virol* **81**: 3685–3692.
35. Rossmann, M.G. (2000). Fitting atomic models into electron-microscopy maps. *Acta crystallographica* **56**: 1341–1349.
36. Rossmann, M.G., Bernal, R., and Pletnev, S.V. (2001). Combining electron microscopic with x-ray crystallographic structures. *J Struct Biol* **136**: 190–200.
37. Adrian, M., Dubochet, J., Lepault, J., and McDowall, A.W. (1984). Cryoelectron microscopy of viruses. *Nature (London)* **308**: 32–36.
38. Carragher, B., Potter, C.S., and Sigworth, F.J. (2007). Software tools for macromolecular microscopy. *J. Struct. Biol.* **157**: 1–288.
39. Wikoff, W.R., Liljas, L., Duda, R.L., Tsuruta, H., Hendrix, R.W., and Johnson, J.E. (2000). Topologically linked protein rings in the bacteriophage HK97 capsid. *Science* **289**: 2129–2133.
40. McPherson, A. (2005). Micelle formation and crystallization as paradigms for virus assembly. *Bioessays* **27**: 447–458.
41. Kuznetsov, Y.G., Zhang, M., Menees, T.M., McPherson, A., and Sandmeyer, S. (2005c). Investigation by atomic force microscopy of the structure of Ty3 retrotransposon particles. *J Virol* **79**: 8032–8045.
42. Kuznetsov, Y.G., and McPherson, A. (2006b). Identification of DNA and RNA from retroviruses using ribonuclease A. *Scanning* **28**: 278–281.